

## Pressure drag in linear and nonlinear quantum fluids

T. Winiecki, J. F. McCann, and C. S. Adams

*Dept. of Physics, University of Durham, Rochester Building, South Road, Durham, DH1 3LE, England.*

(February 27, 2018)

We study the flow of a weakly-interacting Bose-Einstein condensate around an obstacle by numerical solution of the Gross-Pitaevskii equation. We observe vortex emission and the formation of bow waves leading to pressure drag. We compare the drag law with that of an ideal Bose gas, and show that interactions reduce the drag force. This reduction can be explained in terms of a ‘collisional screening’ of the obstacle.

PACS numbers: 03.75.Fi, 67.40.Vs, 67.57.De

A central issue in fluid flow concerns the origin of resistance or drag. In a viscous fluid, shear stresses induced by friction at a surface lead to *skin drag*. In an ideal fluid or superfluid, the effects of shear stress vanish, but normal stresses induced by pressure gradients across an obstacle still produce *pressure drag*.

The recent experimental breakthroughs allowing the production dilute Bose-Einstein condensates [1] has stimulated new interest in the flow and modes of excitation of quantum fluids [2]. Dilute Bose-Einstein condensates are compressible nonlinear quantum fluids, with the attractive feature that the time-evolution can be accurately described by a nonlinear Schrödinger equation (NLSE), known as the Gross-Pitaevskii equation, allowing direct quantitative comparison between theory and experiment [2]. One could envisage an experiment to measure the pressure drag in a dilute Bose-Einstein condensate by studying the flow past an obstacle such as a far-detuned laser beam [3] or a foreign condensate species [4,5]. From numerical solution of the NLSE, it is known that in a uniform flow there is a critical velocity  $v_c$  for the onset of drag [6], however, the drag coefficient and exact dependence on the flow velocity remain unknown.

In this paper, we address these issues by simulating the flow of a weakly-interacting Bose-Einstein condensate around penetrable and impenetrable objects. We show that for a flow velocity  $v$  larger than the critical velocity ( $v > v_c$ ), the drag force varies quadratically with  $v$ , similar to an ideal Bose

fluid. The principle effect of interactions is to reduce drag, which we explain in terms of a ‘collisional screening’ of the object. Also, we show that the effective size of the obstacle is increased due to the healing length of the fluid, and consequently the drag is non-zero even for point-like objects.

The NLSE in a uniform potential may be written as,

$$i\hbar\partial_t\psi = -\frac{\hbar^2}{2m}\nabla^2\psi + V\psi + C|\psi|^2\psi, \quad (1)$$

where the nonlinear coefficient,  $C$ , is determined by the strength of particle interactions, and  $V$  is the object potential. This equation is equivalent to two hydrodynamic equations corresponding to the conservation of mass and momentum, respectively,

$$\partial_t\rho + \partial_i J_i = 0, \quad \text{and} \quad \partial_t J_i + \partial_j T_{ij} = 0, \quad (2)$$

where

$$\rho = m\psi^*\psi, \quad \text{and} \quad J_i = \frac{\hbar}{2i}(\psi^*\partial_i\psi - \psi\partial_i\psi^*), \quad (3)$$

are the mass density and momentum flux, and

$$T_{ij} = \frac{1}{2}\delta_{ij}C|\psi|^4 + \frac{\hbar^2}{4m}(\partial_i\psi^*\partial_j\psi - \psi^*\partial_{ij}\psi + \text{c.c.}), \quad (4)$$

is the stress tensor. The instantaneous drag force on an obstacle is given by

$$F_k(t) = \int_S ds_j T_{jk}(t), \quad (5)$$

where  $S$  defines the surface of the obstacle and  $ds_j$  is an element of  $S$  in the direction of the outward normal. For a linear fluid ( $C = 0$ ) and an impenetrable cylindrical obstacle of radius  $R$ , the drag law may be derived analytically: for high velocity or large object size, ( $v \gg \hbar/mR$ ) the force approaches the classical limit,

$$F = \frac{8}{3}\rho_0 R v^2, \quad (6)$$

where  $\rho_0$  is the background mass density; whereas, for low velocity or small objects ( $v \ll \hbar/mR$ ),

$$F = \alpha(mvR/\hbar)\rho_0\hbar v, \quad (7)$$

where  $\alpha(\zeta) = 16/\pi^2\zeta^2|H_0^{(1)}(\zeta)H_1^{(1)}(\zeta)|^2$  is only weakly-dependent on velocity:  $H_\nu^{(1)}$  is the Hankel function. In this case, often encountered in acoustic scattering, the wave properties dominate and the effective object size is proportional to the wavelength. Inserting  $R \sim \lambda = \hbar/mv$  into Eq. (6), implies  $F \sim \rho_0\hbar v$ , consistent with Eq. (7).

For a weakly-interacting condensate ( $C > 0$ ), the drag force must be evaluated numerically. For the numerical solution, we adopt the reduced units,  $\tilde{t} = t/(\hbar/n_0C)$ ,  $\tilde{y} = y/(\hbar/\sqrt{mn_0C})$ , and  $\tilde{\psi} = \psi/\sqrt{n_0}$ , where  $n_0$  is the in-flow number density. In reduced units, distance  $\tilde{y}$ , and velocity  $\tilde{v}$  are measured in terms of the healing length,  $\xi = \hbar/\sqrt{mn_0C}$ , and the speed of sound,  $c = \sqrt{n_0C/m}$ , respectively; and Eq. (1) becomes

$$i\partial_{\tilde{t}}\tilde{\psi} = -\frac{1}{2}\nabla^2\tilde{\psi} + \tilde{V}\tilde{\psi} + |\tilde{\psi}|^2. \quad (8)$$

This equation is solved in 2D for both penetrable and impenetrable objects [7]. A uniform flow in the  $-y$ -direction is imposed by multiplying the stationary solution by a phase gradient,  $e^{-i\tilde{v}\tilde{y}}$ . In principle, the instantaneous drag force can be determined by numerical integration of the stress tensor at the surface of the obstacle, Eq. (5). However, for impenetrable objects, the finite grid size introduces errors in the differencing approximations to the surface derivatives of  $\psi$ . And for penetrable objects, this procedure is complicated because the fluid-object boundary is ill-defined. The numerical integration can be greatly simplified by recognizing that the time-averaged drag force must be equal to the back-action on the fluid, i.e., the instantaneous force,

$$F_k(t) = -\int_{\Gamma} ds_j T_{jk}(t) - \frac{\partial}{\partial t} \left[ \int_A dA J_k(t) \right], \quad (9)$$

where  $\Gamma$  defines the outer border of a simply-connected region of fluid,  $A$ , encircling the object. The second term, which corresponds to the rate of change of the fluid momentum within  $A$ , averages to zero, if the flow velocity remains constant.

Eq. (9) may be used to calculate the drag for both penetrable and impenetrable objects. Fig. (1) shows a plot of the instantaneous drag,  $F_y(\tilde{t})$ , on an impenetrable cylinder with radius  $\tilde{R} = 5$ , in a flow with velocity  $\tilde{v} = 1.5$ . Initially, the force is dominated by transients which depend on how the flow is turned on. For an instantaneous turn-on,

reflections from the obstacle produce sound waves, which are subsequently absorbed at the edges of the box [7]. However, for longer times the time-averaged drag is independent of the initial conditions. Also, the time-averaged force is independent of the integration path  $\Gamma$ , and for barrier height,  $\tilde{V} > 1$ , only weakly dependent on the penetrability of the obstacle.

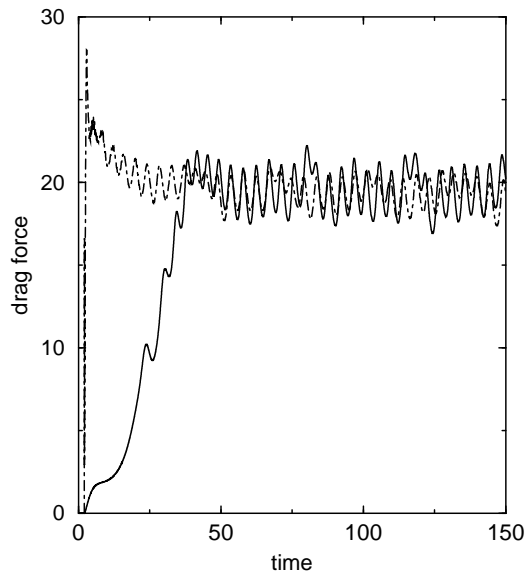


FIG. 1. The instantaneous force,  $F_y$  (in units of  $\hbar\sqrt{n_0^3C/m}$ ), on an obstacle placed in a nonlinear quantum flow with velocity  $\tilde{v} = 1.5$ , as a function of the reduced time,  $\tilde{t}$ . The two curves corresponds to switching on the flow gradually (solid) or instantaneously (dashed). The oscillations are produced by the periodic emission of vortex pairs. Although the instantaneous drag depends on the initial conditions, the time-averaged drag does not.

The oscillatory behaviour of the instantaneous drag is produced by the periodic emission of vortex pairs. The vortex shedding frequency follows from the phase-slip between the main flow and the almost stationary wake behind the obstacle: the wavefunctions for the flow and the wake may be written as  $\tilde{\psi} = e^{-i(1+\tilde{v}^2/2)\tilde{t}}e^{-i\tilde{v}\tilde{y}}$  and  $\tilde{\psi} = \tilde{n}^{1/2}e^{-i\tilde{n}\tilde{t}}$ , respectively, where  $\tilde{n}$  is the mean density behind the obstacle ( $0 < \tilde{n} < 1$ , decreasing at higher velocity). A vortex pair is emitted each time the phase difference accumulates to  $2\pi$ , giving a shedding frequency,  $f = (1+\tilde{v}^2/2-\tilde{n})/2\pi$ . Fig. 2 shows a comparison between the numerical results and the phase-slip model. The shedding frequency lies between the upper and lower limits set by the density, except at low velocity, where the shedding frequency falls to zero.

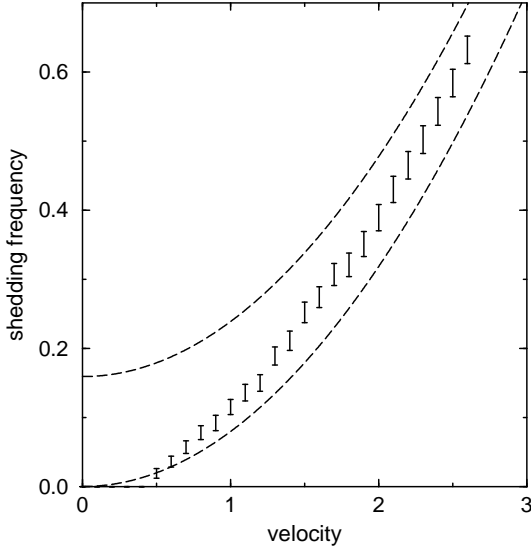


FIG. 2. The vortex shedding frequency,  $f$  (in units of  $n_0 C/\hbar$ ), as a function of the flow velocity,  $\tilde{v}$ . The numerical results lie between the dashed lines,  $\tilde{v}^2/4\pi$  and  $(\tilde{v}^2 + 2)/4\pi$ , which correspond to the upper and lower bounds predicted by considering the phase-slip between the main flow and an almost stationary wake. The error bars reflect the fluctuations in the vortex shedding frequency.

The subsequent motion of the vortices is complex: the first pair is overtaken by subsequent pairs and becomes ‘trapped’ behind the obstacle. However, as apparent in Fig. 1, the vortices do not contribute directly to the time-averaged force, their primary role is to allow the separation of the wake, which then results in a pressure gradient across the obstacle. Fig. 3 shows the time-averaged drag as a function of flow velocity. The error bars correspond to the residual fluctuations after averaging. The drag curve for the linear fluid, Eqs. (6) and (7), is shown as a dashed line. One sees that the main effect of particle interactions is to reduce the drag. Below a critical velocity,  $v_c$ , the drag in the nonlinear fluid falls to zero. In this region, the solutions of the NLSE are time independent and symmetric. The numeric value of  $v_c$  depends on the object shape and penetrability. For an impenetrable cylinder, we find  $v_c = (0.45 \pm 0.01)c$ , consistent with previous work [6,8]. The critical velocity is larger for an impenetrable square barrier, and lower for a penetrable Gaussian object.

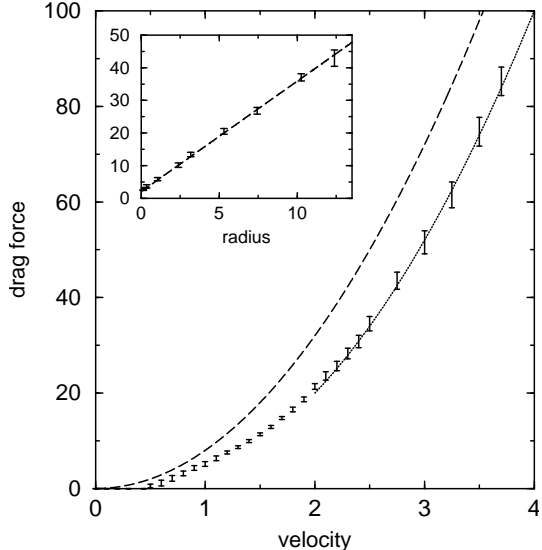


FIG. 3. The time-averaged drag force,  $\overline{F}_y$  (in units of  $\hbar\sqrt{n_0^3 C/m}$ ) as a function of flow velocity,  $\tilde{v}$ , for an impenetrable cylinder with radius  $\tilde{R} = 3$ . The error bars indicate the magnitude of residual fluctuations in the time-averaged drag. The drag law for a linear fluid is indicated by the dashed line. The effect of the non-linearity is to reduce the drag which can be understood in terms of a collisional screening of the object. The reduced drag predicted for a screened object is indicated by the dotted line. The force as a function of the object size for  $\tilde{v} = 1.5$  is shown inset. Note that, the drag is non-zero even for objects much smaller than the healing length.

Above the critical velocity, a pressure drag appears with a velocity dependence similar to the linear fluid. In fact, the force can be predicted accurately by a semi-classical modification of the linear drag law, i.e.,

$$F = \frac{8}{3}\rho_0 R' v'^2, \quad (10)$$

where  $R'$  and  $v'$  are an effective object radius and flow velocity, respectively. A plot of the drag force as a function of object size, Fig. 3(inset), indicates that the effective object size is extended by the healing length  $\xi$  of the fluid. For  $\tilde{v} = 1.5$ , we find that  $R' = R + 0.6\xi$ . An important consequence of this result is that the force does not vanish for small objects,  $R \ll \xi$ , e.g. a point defect in a superconductor.

The effective flow velocity,  $v'$ , may be estimated by considering how the flow is modified by the collisional mean-field. Above the critical velocity, incoming waves are reflected by the obstacle producing a standing wave or bow wave (see Fig. 4), with

a maximum density variation (relative to the background flow) of between  $-n_0$  and  $+3n_0$ . In a semi-classical treatment, an oscillatory potential slows incoming particles by an amount corresponding to half the maximum barrier height, i.e., the effective flow velocity,  $v'^2 = v^2 - \Delta c^2$ , where  $0 < \Delta < 3$ . The dotted line in Fig. 3 is a plot of Eq. (10) using values of  $\Delta$  obtained from the numerical solution. This ‘collisional screening’ model is accurate at high velocity, but less so at lower velocity, where the semi-classical particle treatment begins to break down.

Fig. 4 show a comparison of the time-averaged density distribution for nonlinear (left) and linear (right) quantum fluids. One sees that the finite compressibility of the nonlinear fluid tends to suppress large density fluctuations leading to a smoothing of the standing wave in front of the obstacle. Also far downstream, the direction of the bow waves approaches the Mach angle,  $\alpha = \sin^{-1}(c/v)$ . For the linear fluid,  $c = 0$  and  $\alpha = 0$ , i.e., the bow waves runs adjacent to the geometric shadow behind the obstacle. In the nonlinear fluid, the ‘shadow’ is far less pronounced: the dark streak in the wake, close to the axis of symmetry, corresponds to the vortex street.

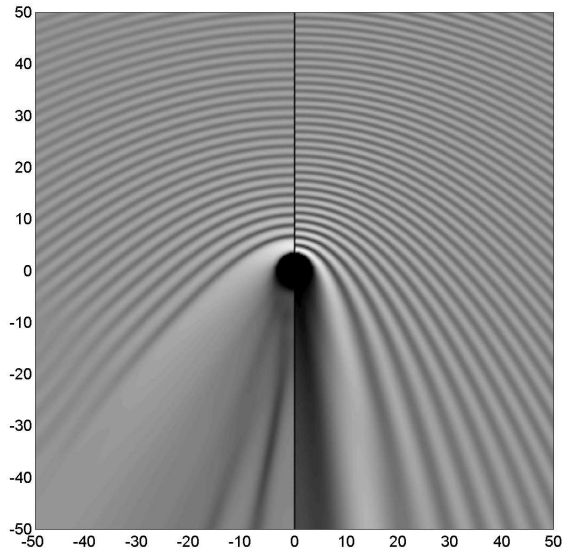


FIG. 4. The time-averaged density distribution for  $\tilde{v} = 2.0$  with (left) and without (right) interactions. The obstacle is an impenetrable cylinder with radius  $\tilde{R} = 3$  centred at the origin, and the flow is from top to bottom. The repulsive particle interactions tend to smooth density variations, thereby reducing the quantum pressure experienced by the obstacle. For the nonlinear fluid (left), the dark line in the wake, close to the axis of symmetry, corresponds to the vortex street.

To summarize, we have solved the NLSE equation in 2D to simulate the flow of a weakly-interacting Bose-Einstein condensate around an obstacle. We observe vortex emission and the formation of bow waves leading to a pressure drag. We find that the drag force is proportional to the screened energy of the flow, and to the object cross-section extended by the effect of fluid healing.

## ACKNOWLEDGMENTS

TW is supported by the Studienstiftung des Deutschen Volkes.

- 
- [1] M. H. Anderson, J. R. Ensher, M. R. Matthews, C. E. Wieman, and E. A. Cornell, *Science* **269**, 198 (1995); K. B. Davis, M. O. Mewes, M. R. Andrews, N. J. van Druten, D. S. Durfee, D. M. Kurn, and W. Ketterle, *Phys. Rev. Lett.* **75**, 3969 (1995); C. C. Bradley, C. A. Sackett, and R. G. Hulet, *Phys. Rev. Lett.* **78**, 985 (1997).
  - [2] F. Dalfovo, S. Giorgini, L. P. Pitaevskii, and S. Stringari, *Rev. Mod. Phys.* (to be published, 1998) also cond-mat/9806038.
  - [3] B. Jackson, J. F. McCann, and C. S. Adams, *Phys. Rev. Lett.* **80**, 3903 (1998).
  - [4] D. S. Hall, M. R. Matthews, J. R. Ensher, C. E. Wieman, and E. A. Cornell, *Phys. Rev. Lett.* **81**, 1539 (1998).
  - [5] B. Jackson, J. F. McCann, and C. S. Adams, preprint.
  - [6] T. Frisch, Y. Pomeau, and S. Rica, *Phys. Rev. Lett.* **69**, 1644 (1992).
  - [7] The time evolution is evaluated using a semi-implicit Crank-Nicholson formula, and applying the split-operator alternating-direction method for spatial differencing. The resulting nonlinear equations are solved using Newton’s method. The calculations were performed using a time step,  $\tau = 0.01$ , and a box size of  $200 \times 200$  healing lengths, divided into  $800 \times 800$  points. The box consists of a central region surrounded by an absorbing border of width 80 points. At the edges, boundary conditions which maintain a uniform flow are applied.
  - [8] C. Huepe and M.-É. Brachet, *C. R. Acad. Sci. Paris*, **325**, 195 (1997).